Visualization of carrier dynamics in p(n)-type GaAs by scanning ultrafast electron microscopy

Jongweon Cho, Taek Yong Hwang, and Ahmed H. Zewail[1]

Physical Biology Center for Ultrafast Science and Technology, Arthur Amos Noyes Laboratory of Chemical Physics, California Institute of Technology, Pasadena, CA 91125

Contributed by Ahmed H. Zewail, January 3, 2014 (sent for review December 24, 2013)

Four-dimensional scanning ultrafast electron microscopy is used to investigate doping- and carrier-concentration-dependent ultrafast carrier dynamics of the in situ cleaved single-crystalline GaAs(110) substrates. We observed marked changes in the measured time-resolved secondary electrons depending on the induced alterations in the electronic structure. The enhancement of secondary electrons at positive times, when the electron pulse follows the optical pulse, is primarily due to an energy gain involving the photoexcited charge carriers that are transiently populated in the conduction band and further promoted by the electron pulse, consistent with a band structure that is dependent on chemical doping and carrier concentration. When electrons undergo sufficient energy loss on their journey to the surface, dark contrast becomes dominant in the image. At negative times, however, when the electron pulse precedes the optical pulse (electron impact), the dynamical behavior of carriers manifests itself in a dark contrast which indicates the suppression of secondary electrons upon the arrival of the optical pulse. In this case, the loss of energy of material's electrons is by collisions with the excited carriers. These results for carrier dynamics in GaAs(110) suggest strong carrier–carrier scatterings which are mirrored in the energy of material's secondary electrons during their migration to the surface. The approach presented here provides a fundamental understanding of materials probed by four-dimensional scanning ultrafast electron microscopy, and offers possibilities for use of this imaging technique in the study of ultrafast charge carrier dynamics in heterogeneously patterned micro- and nanostructured material surfaces and interfaces.

scanning electron microscopy | ultrafast phenomena | charge dynamics imaging

Recent advances in four-dimensional (4D) ultrafast electron microscopy (UEM) have made it possible to investigate nonequilibrium electronic and structural dynamics with atomic-scale spatial resolution and femtosecond temporal resolution (1). Unlike UEM, which operates in the transmission mode, scanning UEM techniques exploit the time evolution of secondary electrons (SEs) produced in the specimen, and provide additional marked advantages over the transmission mode. These include a relatively facile sample preparation requirement, an efficient heat dissipation, a lower radiation damage, and an accessibility to low-voltage environmental study (2, 3). Since its development this technique has been used to study carrier excitation dynamics in several prototypical semiconducting materials surfaces. In these studies, image contrast was monitored as a function of time, and it was found that Si exhibits a bright contrast in the image at positive times without appreciable dynamics at negative times, whereas CdSe displays bright contrast at positive times and dark contrast at negative times (2). However, the correlation between the measured time-dependent SE intensity and electronic structure of the material of interest remains elusive. Chemical doping is a widely used method to control the electronic properties of semiconducting materials by incorporating charge donating or accepting dopant atoms. It is a key element in developments involving modern semiconductor-based solid-state electronics.

Here, we present a systematic study for the doping- and carrier-concentration-dependent carrier dynamics in the in situ cleaved GaAs(110) surface observed in the images obtained using scanning UEM. We show that the enhancement of the SE signal at time 0 is associated with the energy gained by the optical excitation, which increases SE production from the probing pulse, and this process mirrors the electronic doping characteristics of the semiconducting material. In contrast, the persistent dark contrast at both positive and negative times for carrier dynamics in GaAs(110) suggests an energy loss mechanism that involves strong suppression of SEs through carrier–carrier scatterings. Our simulations of the transient behavior further support this conclusion.

A schematic representation of the experimental setup is given in Fig. 1. Electron pulses generated from a field-emission gun using femtosecond laser pulse irradiation are scanned across the specimen surface, which is illuminated with the optical pulse. The electrons emitted from the material surface are used to construct time-resolved images at various time delays between the optical pulse and the electron pulse. The detailed account of the experimental setup was described in previous publications from this laboratory (2–4), and thus here we briefly describe the imaging setup: the laser used in our experiments is an ytterbium-doped fiber laser system that generates ultrashort pulses at a central wavelength of 1,030 nm (measured pulse width of ~400 fs). The second harmonic (photon energy of 2.4 eV) of the laser beam was directed to the sample at room temperature, whereas the quadrupled harmonic (photon energy of 4.8 eV) was used for the pulsed electron generation from the field-emission gun in SEM. For the series of experiments presented here, the pump laser fluence, repetition rate, and the data acquisition methodology were kept the same for comparison of samples with different doping characteristics. The pump laser fluence was deduced to be 69 $\mu J/cm^2$, which is more than three orders of magnitude lower than that reported for the laser-induced damage threshold of a crystalline GaAs (~0.1 J/cm^2 at a photon energy of 1.9 eV)

Significance

Dynamics of positively and negatively charged carriers at surfaces and interfaces plays a fundamental role in a myriad of phenomena, including those involved in the catalysis of chemical reactions and the efficacy of nanoscale devices. However, the visualization of such dynamics in space and time is a nontrivial task. In this contribution we report the methodology for mapping the behavior of such carriers in the semiconductor material GaAs and in two regimes of optical and electron excitation. The technique, which is capable of providing femtosecond temporal resolution and nanometer spatial resolution, has the potential of unraveling phenomena in many other materials and in relating their nature to the electronic structure of matter.

Author contributions: J.C., T.Y.H., and A.H.Z. designed research, performed research, analyzed data, and wrote the paper.

The authors declare no conflict of interest.

[1]To whom correspondence should be addressed. E-mail: zewail@caltech.edu.

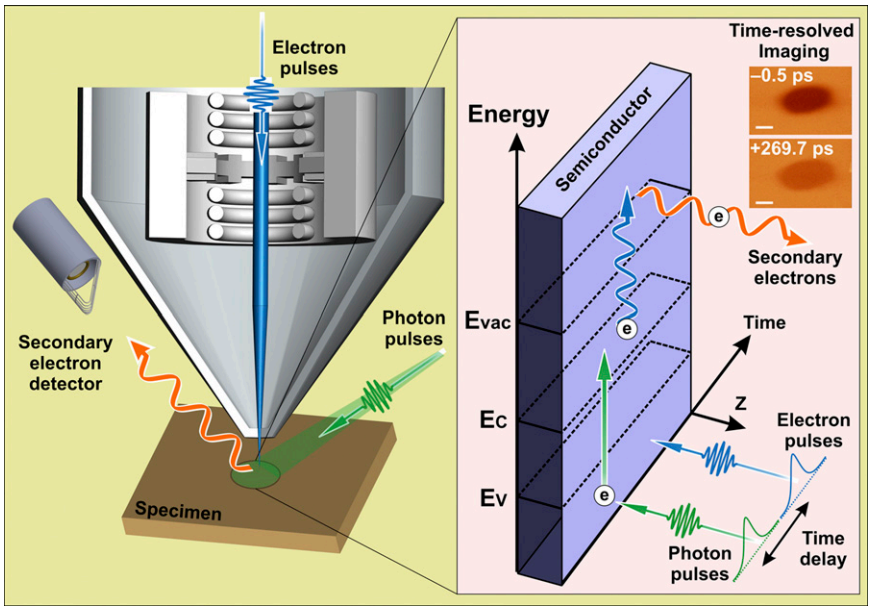

Fig. 1. Schematic representation of the scanning UEM at California Institute of Technology. Pulsed electrons are scanned over a specimen that is illuminated with an optical pulse, and SEs emitted from the material surface are detected to construct time-resolved images at various time delays between the optical and the electron pulse. In the case of a semiconducting material, at time 0, the optical pulse promotes electrons from the valence band to the conduction band, and immediately after that the electron pulse excites transiently populated conduction electrons above the vacuum level, resulting in an enhanced (bright contrast) SE emission. If SEs experience a material-dependent energy loss through the various channels of scattering processes involved while migrating toward the surface, then a decreased emission will result (dark contrast). Here, E_c, E_v, and E_{vac} are the energies of the bottom of the conduction band, the top of the valence band, and the vacuum level, respectively. Scale bars in the time-resolved images correspond to 50 μm.

(5). The emitted electrons from the material were measured using a positively biased Everhart-Thornley detector.

All scanning UEM images were acquired at a dwell time of 1 μs and were integrated 64 times to improve the signal-to-noise ratio. All experiments were conducted at a repetition rate of 4.2 MHz to ensure a full recovery of the material's dynamical response before the arrival of a next pump pulse. Single crystals of GaAs (a direct band gap of 1.43 eV at room temperature) were all grown via Vertical Gradient Freeze method (purchased from MTI); the method is known to produce fewer defects during the growth, compared with those grown via the liquid encapsulated Czochralski method (6). The crystals were in situ cleaved in high vacuum ($<1.5 \times 10^{-6}$ Torr) to reduce the effects of contamination and formation of surface defects or adsorbates for the systematic study presented here. A clean (110) crystallographic orientation of GaAs does not possess any surface states within the band gap and thus a bulk-like band structure is expected at the surface without band-bending effects (7, 8). Cleavage along a direction perpendicular to the (001) orientation of GaAs exposes a fresh (110) plane. The cleaved surface was positioned at a working distance of 10 mm and perpendicular to the propagation direction of the pulsed primary electron beam with its energy of 30 keV.

Results and Discussion

Fig. 2 shows the difference images in which SEM images acquired at far negative time were subtracted from the images acquired at different time delays for doped and undoped GaAs (110) surfaces. There are three common dynamical features for all of the investigated GaAs(110) samples: development of dark contrast at negative times, followed by an ultrafast stepwise increase in the SE signal at time 0, and then a decay which reflects the relaxation of carriers toward equilibrium. We note that the measured contrast here at both negative and positive times is of dark nature, in marked difference from the previously investigated semiconductors such as Si and CdSe (2). These differences are correlated with changes in the electronic structure, as will be discussed later.

In general, we have recorded SE signals from the most intense part of the illuminated sample area and the acquired images were obtained as a function of the time delays between the pulsed photons and electrons. First, however, we characterized our experimental response function on a single-crystalline Si surface to determine the temporal resolution and overall instrumental response when the electron pulse train is generated with the UV excitation at 257 nm. Fig. 3*A* displays the SE signals acquired from n-type Si(100) samples under the identical experimental conditions used for the GaAs study except for the pump laser fluence, ~1 mJ/cm^2. For Si(100) we observe an emergence of a bright contrast near time 0 (2), with a rise time of 2.7 ± 0.7 ps from a 4-nJ electron-generating pulse. Time 0 determined from the sigmoidal fit in this Si carrier dynamics was used for the GaAs study (2).

In Fig. 3 *B* and *C* we display the SE signals extracted from the center of the laser excitation footprint on GaAs(110) samples which possess different electronic structures. In Fig. 3*B* the SE intensities are normalized to their minimum values and the error bars indicate the SD of the intensities obtained from different measurements on different samples. There are some distinct features in the measured SE intensities, which depend on the level of chemical doping and the concentration. First, the magnitude of the intensity increases at time 0 and exhibits its strong dependence on doping. Fig. 3*B* (*Inset*) shows the doping-dependent intensity enhancement at time 0. For n-type GaAs(110) the enhancement is the largest, whereas for p-type GaAs(110) it is the smallest. For undoped GaAs(110) the magnitude of the enhancement remains between those for n-type and p-type. It is noteworthy that there is an additional spike-like feature near time 0. Second, the time scale of carrier relaxation at positive times is also doping-dependent. In addition to a nanosecond-scale relaxation time, reflecting electron–hole recombination (9), there are picosecond time-scale components with time constants of 207 ± 131 ps

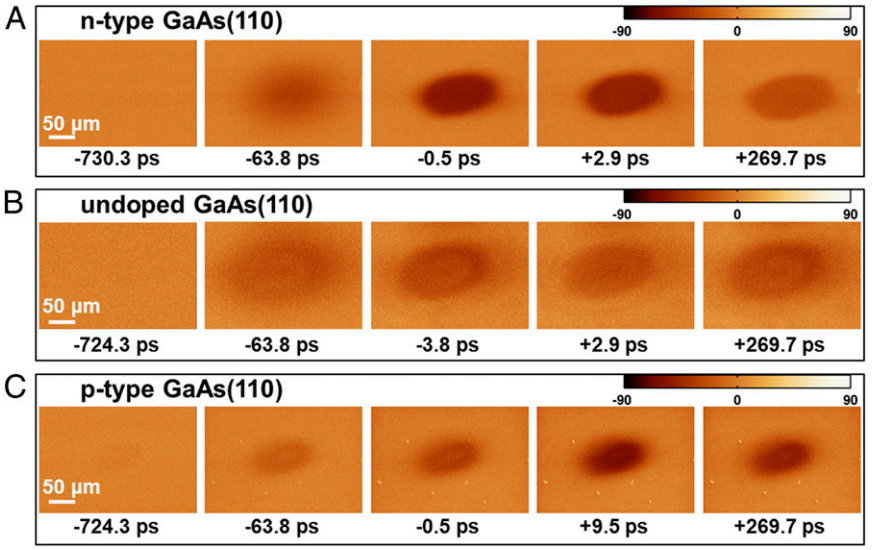

Fig. 2. Time-resolved scanning UEM images of p-type, n-type, and undoped GaAs. The difference images were obtained by subtracting the images acquired at (far) negative time (where the measured transient response was negligible) from the images acquired at the indicated time delay: (*A*) n-type, (*B*) undoped, (*C*) p-type GaAs(110). The carrier concentrations are (7.1–7.4) $\times$ 10^{17} cm^{-3} for n-type, (5.3–5.6) $\times$ 10^{17} cm^{-3} for p-type, and 1.8 $\times$ 10^{6} cm^{-3} for undoped GaAs (110), respectively.

and 39 $\pm$ 17 ps for n-type and p-type GaAs(110), respectively, when the signals are fitted to an exponential decay function. Lastly, the dynamical behavior of charge carriers at negative times displays a strong dependence on chemical doping. The best fit, assuming an exponential function, yields time constants of 95 $\pm$ 3 ps and 90 $\pm$ 3 ps for undoped and n-type GaAs(110), respectively. For p-type GaAs(110) the best fit, using a biexponential function, yields time constants of 233 $\pm$ 34 ps and 18 ps.

Before discussing the behavior in the three time ranges, it is worth noting that the SE intensity plots shown in Fig. 3 represent the difference images, where the SE intensities for the unilluminated areas have already been subtracted. The temporal evolution of the SE intensities observed at various time delays must reflect dynamics arising from the material in response to photoirradiation, as the intensities acquired from the unilluminated areas do not exhibit such dynamics in the difference images, as shown in Fig. 2. In the following, we will discuss the dynamics observed for three temporal regimes: time 0, negative times, and positive times.

Behavior at Time Zero

Doping-dependent enhancement at time 0 is the largest in magnitude for n-type and the smallest for p-type GaAs(110), and could, in principle, be attributed either to differences in (*i*) optical absorption or to (*ii*) nonequilibrium transient population of conduction band electrons. Because the difference in optical absorption with doping is expected to be insignificant at the used excitation photon energy of 2.4 eV, which is far from the absorption edge excitation (10), we rule out the former (*i*). At time 0, the femtosecond optical pulse with a photon energy above the band gap initiates excitation of electrons from the valence band into the conduction band. The electron pulse immediately changes the population of the photoexcited electrons in the conduction band. Consequently, these electrons in the conduction band acquire a higher probability of SE emission, because they experience a lower apparent energy barrier to overcome for detection compared with the ones without the optical pulse. This energetic preference (energy gain) leads to the sharp enhancement in our measured signal at time 0.

The intensity increase from the minimum value is consistent with the equilibrium electronic band structure of GaAs (11). Fig. 4*A* displays a single-electron picture in schematic energy-level diagrams, illustrating the population difference with different doping characteristics, in accord with the energy gain mechanism described above. As the difference in the optical absorptions for the three doping levels is negligible at the 2.4-eV pump excitation, this doping-dependent enhancement arises from the differences in photoassisted energy gain associated with the energy distribution of optically excited transiently populated conduction electrons upon the arrival of the electron pulse. For n-type GaAs, the electrons are at a donor level located close to the conduction band minimum with a high density of states; they will be promoted to the conduction band upon absorption of the photon. For p-type GaAs, the photoexcited electrons are located energetically far from the vacuum level, compared with n-type GaAs, owing to the position of the acceptor level which is close to the valence band maximum. During the subsequent thermalization process (within a couple of picoseconds) (12) the photoexcited charge carriers redistribute within the conduction band through carrier–carrier scatterings and carrier–phonon scatterings, and the number of photoexcited charge carriers would not be altered. Differences in the transient population distribution of electrons in the conduction band arise because no two electrons can occupy the same quantum state, the Pauli exclusion principle: thermalized photoexcited electrons for n-type fill energy levels in the conduction band to higher energies compared with those for p-type. This effectively leads to the doping-dependent energy gain, which contributes to a different enhancement at the time 0, as seen in our data.

Our experimental observations with different carrier concentrations of n-type GaAs(110) corroborate the above interpretation. As we increase the carrier concentration of the material, the transient population of conduction band electrons favors a relatively large energy gain, resulting in a higher efficiency in the dynamic SE emission. The enhancement of the SE signal measured at time 0 increases with the increase in carrier concentration, as shown in Fig. 3*C*. The spike-like feature for the undoped GaAs(110) shown in Fig. 3*B* may be associated with either (*i*) the presence of surface defects or adsorbates (at the vacuum condition used) or (*ii*) strain induced during the in situ cleavage process, as this spike-like feature largely varies for different undoped samples, compared with the investigated

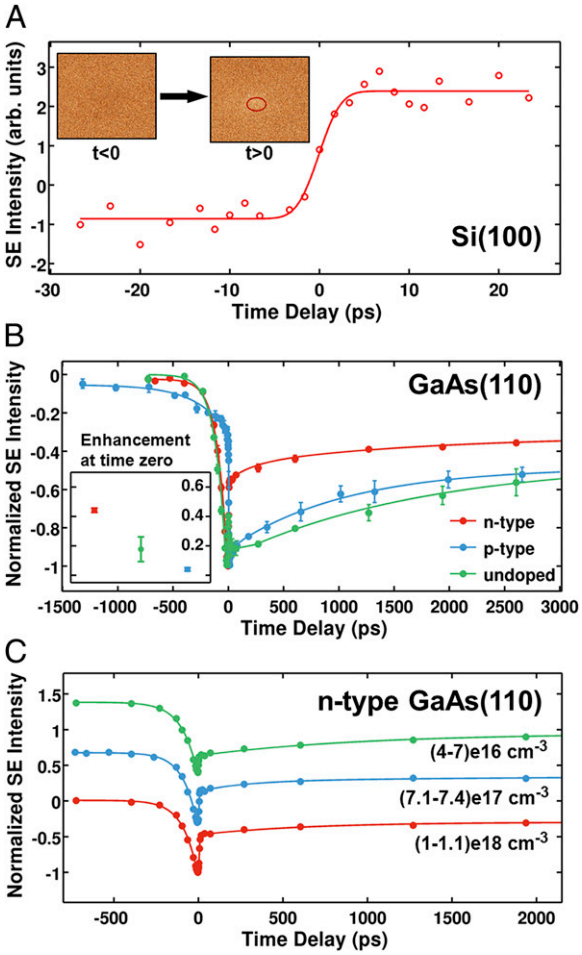

Fig. 3. Ultrafast dynamics of p-type, n-type, and undoped GaAs. (*A*) Ultrafast carrier dynamics in n-type Si(100) for characterization of the system response. (*Inset*) Difference images acquired at the time before and after time 0, referenced to an image acquired at (far) negative time. The sigmoidal fit yields a rise time of 2.7 ± 0.7 ps when UV 257-nm pulses were used for the electron pulse generation. (*B*) Doping-dependent SEs acquired for up to 3 ns. The intensities are extracted from the most intense part of the illuminated area of the difference image, as shown in Fig. 2, and then normalized to their minimum. The carrier concentrations are $(7.1–7.4) \times 10^{17}$ cm^{-3} for n-type, $(5.3–5.6) \times 10^{17}$ cm^{-3} for p-type, and 1.8×10^{6} cm^{-3} for undoped GaAs(110), respectively. (*Inset*) Intensity enhancement measured at time 0, which is extracted from the main plots. (*C*) Normalized SEs of n-type with different carrier concentrations, following the same procedure as in *B*. Note that the intensities have been shifted vertically for clarity. Solid lines are drawn as guides to the eye.

doped GaAs samples. We note that the former case (*i*), if dominant, may give rise to electronic states pinned near the Fermi level within the band gap, whereas the gap for a clean, cleaved GaAs surface is free of surface states (8, 9). The electrons occupying these states will be excited upon the absorption of a photon, and these surface defects are likely to serve as charge traps through free-to-bound transitions (9) during carrier relaxation processes, resulting in prompt reduction in the SE intensity and thus the appearance of a spike-like feature.

Behavior at Negative Times

We now turn to a discussion of the carrier dynamics at negative times. In this case, the dynamics is that of an electron impact, where the material nonequilibrium response initiated by the primary electron pulse is transiently altered by the subsequent optical pulse. Observing dark contrast thus indicates that the optical pulse suppresses the SEs that leave the surface of the material; see Fig. 4*B* for illustration. Whereas it has been commonly accepted that the majority of SEs which escape are created within a shallow region from the surface (13), an impinging electron pulse also creates internal SEs within the material which then lose their excess energy, due to carrier–carrier and carrier–phonon scatterings, as they migrate toward the surface to escape. In the absence of the optical excitation the energy loss may be schematically shown in Fig. 4*B* by the dotted–dashed line. With optical excitation, the internal SEs may encounter additional energy loss on their way to the surface mainly through inelastic electron–electron, electron–phonon, and electron–impurity scatterings. The time scales for these three processes are different and such time scales determine the efficiency of events involved; electron–electron scatterings occur in tens of femtoseconds (12), whereas electron–phonon scatterings take place in a few picoseconds, primarily involving emission of longitudinal optical phonons with an energy of 37 meV (14). Electron–impurity scatterings involve carrier traps and/or recombinations; such processes will occur on a slower time scale than that of electron–electron scatterings and their rates will depend on the level of doping in the material. The important point to recall is that these energy loss processes cause a downward shift in the low-energy (tail) of the probability distribution of emitted SEs, resulting in a decrease in the number of electrons, and hence the dark contrast observed experimentally.

Consistent with the above findings is the effect of doping. The distinctly different dynamical behavior of charge carriers for n-type and p-type GaAs(110) at negative times is accounted for because Si was used for n-type and Zn for p-type. For the p-type, the observed (18 ps) component appearing at negative times reflects this difference in the scattering properties of SEs when Si- and Zn-doped GaAs are studied. In the case of Zn, it is expected that the electron penetration depth becomes smaller by ∼40% and the elastic scattering rate becomes larger by a factor of about 5 than those for Si (15, 16), resulting in the near-the-surface faster dynamics at negative times. It follows that the interplay of the electron penetration depth and scattering rates, which depend on differences in the atomic number of the dopant, determines the electron-impact dynamics at negative times, consistent with our experimental observation of the faster time response when Zn-doped GaAs was examined.

Behavior at Positive Times

At positive times, the material is excited by the optical pulse and probed with the electron pulse. First, we excluded the effect of thermal excitation, as the maximum lattice temperature rise at the center of illuminated zone is estimated to be ∼2 K for the fluence used; when the material temperature was increased no sign of the dark contrast was observed. The observed behavior is due to the nonthermal optical excitation. The absorption of photons first creates electron–hole pairs across the band gap, yielding the increase in the electron population in the conduction band. Upon impingement of an electron pulse, these conduction electrons are promoted above the vacuum level with appreciable energy gain (on the order of energy gap), giving rise to an overall enhancement for the probability of SE emission. As such, one should observe bright contrast at positive times; see Fig. 4*C*, green dotted line. However, if SEs are immediately subjected to the scattering processes discussed above, then a decrease in SEs will give rise to dark contrast; see Fig. 4*C*, green solid line. The effective cross-section for the scattering of internal SEs with conduction electrons is expected to be higher than that with valence electrons because there are fewer allowed electronic states for valence electrons due to the presence of the band gap. Moreover, the phase-space constraint to fulfill both energy and momentum conservation for these scattering processes is less stringent compared with, for instance, that for intra- and interband electron–electron scattering events taking place within the conduction

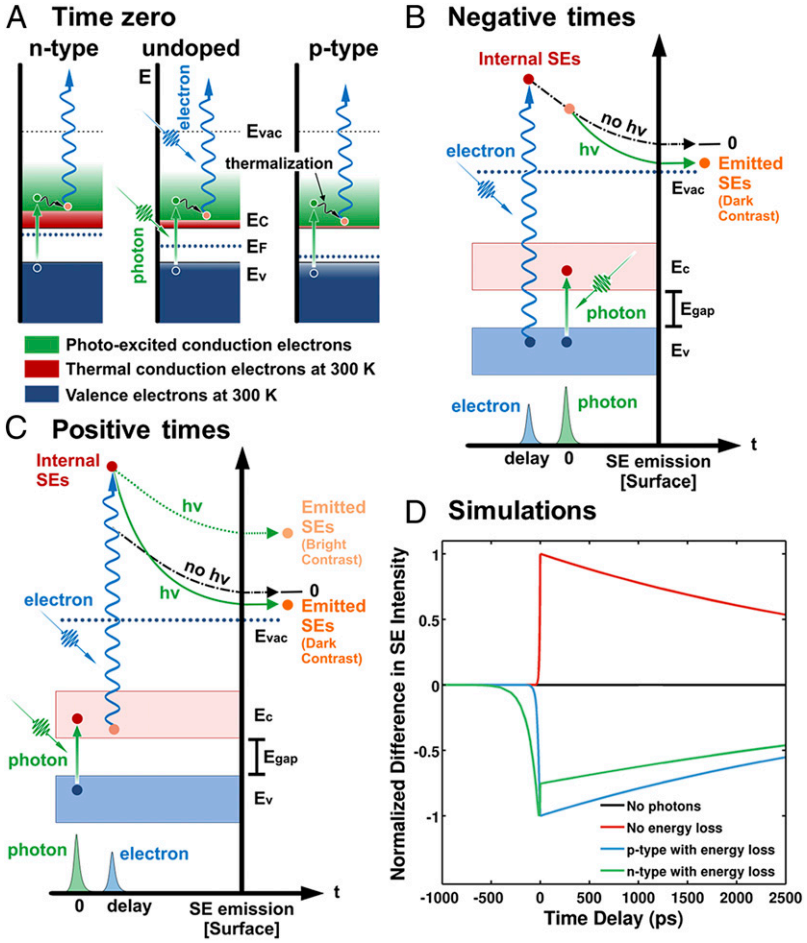

Fig. 4. Energy-level pictures and transient simulations. (*A*) Single-electron picture in a simple flat band diagram to illustrate origin of the intensity enhancement for carrier dynamics at time 0. As the optical absorptions for the three doping levels are similar at the 2.4-eV pump excitation, this doping-dependent enhancement stems from the differences in photoassisted energy gain associated with the energy distribution of optically excited transiently populated conduction electrons upon the arrival of the electron pulse, which depends on chemical doping and doping concentration at equilibrium. Thermalized transient conduction electrons after optical excitation, thermal conduction electrons, and valence electrons at room temperature are indicated by green, red, and blue blocks, respectively (populations are not to scale). (*B*) Single-electron picture to account for the observed carrier dynamics of GaAs(110) at negative times. (*C*) Single-electron picture for the carrier dynamics at positive times. In *B* and *C*, the energy-loss behavior of the material's SE in the absence of the optical pulse is indicated by the black dotted–dashed line, whereas the transient SE trajectory when the photoinduced energy loss mechanisms are operative is indicated by the green solid line (dark contrast). No contrast in difference images is shown as 0. The green dotted line in *C* denotes the transient SE trajectory when the additional energy loss mechanisms are inefficient (bright contrast). (*D*) Simulation results based on a coupled rate-equation model (see the detailed discussion in *Simulations of Transient Behaviors*). Black and red plots indicate the simulated SE intensities in the absence of optical pumping and the additional photoinduced SE energy loss mechanism (predominantly inelastic electron–electron scatterings), respectively. Blue and green plots indicate the simulated intensities for p-type and n-type GaAs, when the SE energy loss mechanisms are taken into account.

band, because there are many allowed states present in the continuum in the course of energy loss for the internal SEs. Therefore, the material-dependent energy gain or energy loss of SEs will result in either bright or dark contrast at positive times. In stark difference to the dynamical behavior of Si (bright contrast at positive times and no dynamics at negative times) and CdSe (bright contrast at positive times and dark contrast at negative times) (2), carrier dynamics in GaAs(110) exhibits persistent dark contrast at both positive and negative times. Such sensitivity to doping levels and scattering channels are the basis for the potential of this technique in the study of materials charge distribution and transport.

As shown in Fig. 3*C*, the dynamics at time delays far from time 0 appears to be quite similar and less distinct. This asymptotic behavior reflects the balance between energy gain and energy loss. Energy gain in electron pulse excitation involves a fraction of photoexcited carriers and consequently the remaining carriers serve as scattering sources contributing to energy loss, which results in an effective reduction in the carrier concentration dependence.

Simulations of Transient Behaviors

To get further insights we performed numerical simulations of transient electron populations in the semiconductor which result in SE emission. Because coherence effects are absent on the time scales reported here, it is appropriate to invoke coupled rate equations (17). Three energy bands will be considered:

$$\frac{dN_1}{dt} = \Lambda_{21} N_2 + \Lambda_{31} N_3 - \Gamma_{ee} N_1 - \Gamma_{ep} N_1 - \Gamma_{ei} N_1,$$

$$\frac{dN_2}{dt} = -\Lambda_{21} N_2 + \Gamma_{ee} N_1 + \Gamma_{ep} N_1 + \Lambda_{32} N_3 + \Lambda_{ph} N_3 - \Gamma_{eh} (N_2 - N_{20}),$$

$$\frac{dN_3}{dt} = -\Lambda_{32} N_3 - \Lambda_{31} N_3 - \Lambda_{ph} N_3 + \Gamma_{eh} (N_2 - N_{20}).$$

Here N_1, N_2, and N_3, respectively, are the effective population of the internal SEs (above vacuum level), the conduction band electrons, and the valence band electrons. Λ_{ij} (i = 1, 2, 3, j = 1, 2) denotes an electron-pulse-induced pumping rate of population from N_i to N_j. Λ_{ph} represents an optically induced pumping rate of population from N_3 to N_2, which includes the laser fluence used in the experiment. Γ_k ($k = ee, ep, ei$) denotes a population decay rate via the aforementioned scattering mechanisms responsible for energy loss: inelastic electron–electron interactions (Γ_{ee}), electron–phonon scattering (Γ_{ep}), and electron–impurity scattering (Γ_{ei}). Lastly, Γ_{eh} is the carrier relaxation through electron–hole recombination, and N_{20} is the conduction band electron population at thermal equilibrium.

For simplicity, we made a few assumptions regarding the parameters used, which allowed us to qualitatively reproduce the transient SE behavior. Considering all of the SE generation processes within the material resulting from the Gaussian-shaped electron pulse excitation, we first assume that Λ_{ij} can be represented as a single exponential decay, $\Lambda_{ij} = \Lambda_{ij0} \exp[-\Gamma_0\ (t-t_0)]$ $H(t-t_0)$, where t_0 is the time delay between the electron pulse and the optical pulse, $H(t)$ is the Heaviside step function, and Γ_0 is its effective decay rate. To adequately treat the energy dependence of the electron pumping rate, Λ_{ij0} in this expression is further assumed to decrease with the increase in the difference between the two energy levels involved in the population transition.* Moreover, we stress that mutual electron–electron and electron–impurity scattering rates are nonlinear in nature and thus we only consider its leading order for the sake of tractable analysis: now $\Gamma_{ee} = \kappa_{ee}\ N_2$ and $\Gamma_{ei} = \kappa_{ei}\ N_{imp}$, where κ_{ee} and κ_{ei} are constant coefficients that depend on the collisional transition strength of SEs with N_2 and impurity concentration, N_{imp}, respectively.

The simulated electron emission intensity in the present model is determined by the integral of the SE population from a specific time delay to infinity:

$$N_{SE}(t_0) \propto \int_{t_0}^{\infty} dt\, N_1(t).$$

The key parameters responsible for the temporal evolution of emitted SE intensities are relative interaction strength among Γ_k ($k = ee, ep, ei$) and Λ_{21}.

Fig. 4*D* shows the simulation results that provide a qualitatively consistent explanation for our experimental data. First, when photons are absent, no dynamics is seen, as indicated by a black flat line. Second, when photons are present but the additional SE energy loss mechanism predominantly arising from inelastic electron–electron scattering is not operative, we only expect to observe bright contrast at positive times without any appreciable dynamical behavior at negative times (red line). Finally, when photons are present and the additional energy loss mechanisms are operative, along with the previously described dopants dependence, the simulation results yield the intensity enhancement and the carrier relaxation behaviors as indicated by green and blue lines, confirming the systematic trend of carrier dynamics for n-type and p-type GaAs(110) observed in our data.

Concluding Remarks

In this contribution, using 4D scanning UEM, we have investigated the electronic properties of GaAs(110) for different types (p and n) and at different dopant concentrations. We identified two physical mechanisms that are controlled by the electronic structure and the material's composition. On one hand, photo-assisted energy gain for SE emission can give rise to bright contrast, whereas electron-impact-type excitation, followed by optical excitation, can hinder SE emission and lead to dark contrast. These findings offer the link between the measured transients and the electronic structure of materials under study, and provide the means to study new surfaces such as those of photovoltaic cells or micro- and nanofabricated structures.

ACKNOWLEDGMENTS. This work was supported by the National Science Foundation Grant DMR-0964886 and the Air Force Office of Scientific Research Grant FA9550-11-1-0055 for research conducted in The Gordon and Betty Moore Center for Physical Biology at the California Institute of Technology.

*We verified that a similar transient behavior is attainable for the emitted SE, as shown in Fig. 4*D* via the simulations, with a power-law decay of $\Lambda_{ij\,0}$, $|E_i - E_j|^n$, $n = -1, -2$ (used in Fig. 4*D*), and -4.

1. Zewail AH (2010) Four-dimensional electron microscopy. *Science* 328(5975):187–193.
2. Mohammed OF, Yang DS, Pal SK, Zewail AH (2011) 4D scanning ultrafast electron microscopy: Visualization of materials surface dynamics. *J Am Chem Soc* 133(20): 7708–7711.
3. Yang DS, Mohammed OF, Zewail AH (2013) Environmental scanning ultrafast electron microscopy: Structural dynamics of solvation at interfaces. *Angew Chem Int Ed Engl* 52(10):2897–2901.
4. Yang DS, Mohammed OF, Zewail AH (2010) Scanning ultrafast electron microscopy. *Proc Natl Acad Sci USA* 107(34):14993–14998.
5. Kim AMT, Callan JP, Roeser CAD, Mazur E (2002) Ultrafast dynamics and phase changes in crystalline and amorphous GaAs. *Phys Rev B* 66(24):245203.
6. Szweda R (2000) *Gallium Arsenide, Electronics Materials and Devices* (Elsevier, New York), 3rd Ed.
7. Feenstra RM, Stroscio JA (1987) Tunneling spectroscopy of the GaAs(110) surface. *J Vac Sci Technol B* 5(4):923–929.
8. Zangwill A (1988) *Physics at Surfaces* (Cambridge Univ Press, New York).
9. Yu P, Cardona M (2005) *Fundamentals of Semiconductors* (Springer, Berlin), 3rd Ed.
10. Casey HC, Sell DD, Wecht KW (1975) Concentration-dependence of absorption-coefficient for n-type and p-type GaAs between 1.3 and 1.6 eV. *J Appl Phys* 46(1):250–257.
11. Cavassilas N, Aniel F, Boujdaria K, Fishman G (2001) Energy-band structure of GaAs and Si: A sps* k•p method. *Phys Rev B* 64(11):115207.
12. Sundaram SK, Mazur E (2002) Inducing and probing non-thermal transitions in semiconductors using femtosecond laser pulses. *Nat Mater* 1(4):217–224.
13. Seiler H (1983) Secondary-electron emission in the scanning electron-microscope. *J Appl Phys* 54(11):R1–R18.
14. Blakemore JS (1982) Semiconducting and other major properties of gallium-arsenide. *J Appl Phys* 53(10):R123–R181.
15. Kanaya K, Okayama S (1972) Penetration and energy-loss theory of electrons in solid targets. *J Phys D Appl Phys* 5(1):43–58.
16. Reimer L (1998) *Scanning Electron Microscopy: Physics of Image Formation and Microanalysis* (Springer, Berlin), 2nd Ed.
17. Svelto O (1998) *Principles of Lasers* (Springer, New York), 4th Ed.